Experimental study on flexural capacity of near-surface mounted FRP reinforced concrete beams

Experimental study on flexural capacity of near-surface mounted FRP reinforced concrete beams

Cristina Barris Peña[*, a], Carlos Lores Catalán[b], Younes Jahani[c], Marta Baena Muñoz[d] y Lluís Torres Llinàs[e]

[a] Associate Prof. Dr. Dept. Mech. Engineering and Industrial Construction, AMADE research group, Universitat de Girona, Spain

[b] Msc. Civil Engineer, AMADE research group, Universitat de Girona, Spain

[c] Msc. Civil Engineer AMADE research group, Universitat de Girona, Spain

[d] Associate. Prof. Dr. Dept. Mech .Engineering and Industrial Construction, AMADE research group, Universitat de Girona, Spain

[e] Prof. Dr. Dept. Mech .Engineering and Industrial Construction, AMADE research group, Universitat de Girona, Spain

RESUMEN

Se presentan los resultados experimentales de veintisiete vigas de hormigón armado reforzadas con materiales compuestos empleando la técnica de refuerzo inserido en el recubrimiento ensayadas en la Universitat de Girona. Su capacidad flexión se comprueba con un análisis teórico seccional, observando que en la mayoría de los casos, los especímenes no alcanzan su capacidad última a flexión debido a problemas de adherencia. A continuación, se emplean las metodologías descritas en ACI 440.2R-17, en CSA S806-12 y por Zilch para predecir la carga de fallo por adherencia. Se observa que los métodos de ACI y Zilch proporcionan valores conservativos para la capacidad máxima de las vigas.

ABSTRACT

This paper presents the experimental results on the flexural capacity of twenty-seven reinforced concrete beams strengthened with Near-Surface Mounted (NSM) Fibre Reinforced Polymer (FRP) reinforcement carried out at the Universitat de Girona. The resultant experimental flexural capacity is analysed through sectional analysis, obtaining that in most of the beams the full flexural capacity is not attained due to premature debonding. The theoretical provisions of ACI 440.2R-17, CSA S806-12 and a methodology proposed by Zilch et al. considering debonding failure are analysed. The results indicate that, in general, ACI and Zilch et al. approaches give conservatives values for the maximum load capacity.

PALABRAS CLAVE: materiales compuestos (FRP), NSM., flexión, adherencia.
KEYWORDS: fibre reinforced polymers (FRP), NSM, flexural behaviour, bond.

1. Introduction

Strengthening of reinforced concrete (RC) structures with fibre reinforced polymers (FRP) has been proven to be successful methodology to increase the load carrying capacity of flexural members [1–3]. Two main techniques are found: the externally bonded (EB) reinforcement, in which a FRP plate is bonded tot the tensile face of the RC beam, and

the near-surface mounted (NSM) technique, where the FRP reinforcement is inserted into a groove previously cut in the concrete cover. In general, NSM technique presents better bond performance and higher protection against external exposure. Preventing debonding between FRP and concrete substrate is a crucial aspect when designing FRP flexural strengthening of RC elements [4,5]. Several design guidelines and codes provide a first generation of simplified formulations in order to prevent or predict premature failure of NSM or EB FRP RC beams due to debonding [3,6–8].

In this paper, the experimental results of 27 RC beams strengthened with NSM FRP in 4-point bending loading, are presented and analysed. The experimental flexural capacity and failure mode of all specimens are analysed and compared with predictions of three different approaches: i) the Canadian code CSA S806-12 [8], ii) the American guideline ACI 440.2R-17 [6], and iii) the formulation developed by Zilch et al. [9].

2. Experimental programme

The experimental results shown in this work are part of four different experimental programmes carried out at the University of Girona, being S-1 unpublished results, whereas those of S-2, S-3 and S-4 can be found in [10–12]. Details on beam specimens are found in Table 1 and Figure 1.

Table 1. Experimental programmes Campaigns and specimens' main characteristics

Series	N. beams	UN	CFRP	GFRP	L (mm)	L_1 (mm)	a (mm)	b (mm)	h (mm)	d (mm)	f_c (MPa)	f_y (MPa)
S-1	**12**	1	9	2	2100	500	150	140	180	146	35.0	515
S-2	**8**	1	3	4	2400	800	200	160	280	236	32.4	540
S-3	**2**	-	2	-	2400	800	200	160	280	236	31.9	540
S-4	**5**	2	3	-	2100	700	150	140	180	146	33.0	515

In Table 1, L is the distance between supports, L_1 is the shear span, a is the distance between the support and the laminate, b and h are the width and height of the section respectively, d is the effective depth, f_c is the concrete strength and f_y is the steel yield strength, whilst UN stands for the number of unstrengthened beams, and CFRP and GFRP for beams strengthened with these two types of FRP reinforcement.

The main parameters of the different programmes were the type of reinforcing material, the sectional dimensions, the internal and external reinforcing ratio and different lengths (L, L_1).

The concrete strength and the steel yield strength of materials used in each programme are specified in Table 1, whilst the reinforcing and geometrical details of each specimen are summarised in Table 2. The type (bar or strip), type of fibre, surface coating and mechanical properties of the FRP materials are also included in Table 2.

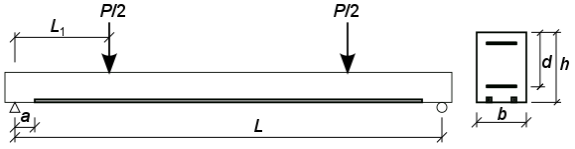

Figure 1. Test setup for the different experimental programmes

Table 2. Details of NSM and internal reinforcement for specimens

	Specimen	FRP Type	FRP Fibre	E_{fu} (GPa)	A_f (mm²)	d_f (mm)	A_{s1} (mm²)	d_{s1} (mm)	A_{s2} (mm²)	d_{s2} (mm)
S-1	**R**	-		-	-	-	157	147	57	26
	C1-1L	Strip	Carbon	160	14	172	157	147	57	26
	C1-2L	Strip	Carbon	160	28	172	157	146	57	26
	C1-4L-2G	Strip	Carbon	160	56	172	157	147	57	26
	C1-4L-3G	Strip	Carbon	160	56	172	157	146	57	26
	C2-1L	Strip	Carbon	169	30	172	157	146	57	26
	C2-2L	Strip	Carbon	169	60	172	157	147	57	26
	C3-3L	Strip	Carbon	169	90	172	157	146	57	26
	C1-1B8	Bar	Carbon	155	201	172	157	146	57	26
	G1-1B8	Bar	Glass	60	402	172	157	146	57	26
	C1-2B8	Bar	Carbon	155	201	172	157	146	57	26
	G1-2B8	Bar	Glass	60	402	172	157	147	57	26
S-2	**CB**	**-**		-	**-**	**-**	226	236	101	42
	LB1C1	Bar	Carbon	170	201	272	226	236	101	42
	LB1G1	Bar	Glass	64	201	272	226	236	101	42
	LB2C1	Bar	Carbon	170	402	272	226	236	101	42
	LB2G1	Bar	Glass	64	402	272	226	236	101	42
	LA2C1	Bar	Carbon	170	402	272	226	236	101	42
	LA2G1	Bar	Glass	60	402	272	226	236	101	42
	LB1G2	Bar	Glass	60	452	268	226	236	101	42
S-3	**LB2S1**	Strip	Carbon	165	56	272	226	236	101	42
	LB4S2	Strip	Carbon	165	112	267.5	226	236	101	42
S-4	**R1**	-	-	-	-	-	157	146	57	26
	S1-2F	Strip	Carbon	160	28	172	157	146	57	26
	S1-4F	Strip	Carbon	160	56	172	157	146	57	26
	R2	-	-	-	-	-	402	146	157	26
	S2-2F	Strip	Carbon	160	28	172	402	146	157	26

3. Flexural capacity: experimental results vs. theoretical predictions according to a sectional analysis

In this section, the experimental results of all beams are compared to the theoretical sectional flexural capacity assuming the Bernoulli hypothesis (plain sections before bending remain plain after deformation), fully-cracked section and perfect bond among materials. The parabola-rectangle curve from Eurocode-2 [13] has been adopted for modelling concrete behaviour. Elastic-plastic behaviour for steel and linear stress-strain relationship until failure for FRP have been assumed.

The moment capacity is obtained from sectional compatibility of deformations and equilibrium of forces, according to Figure 2.

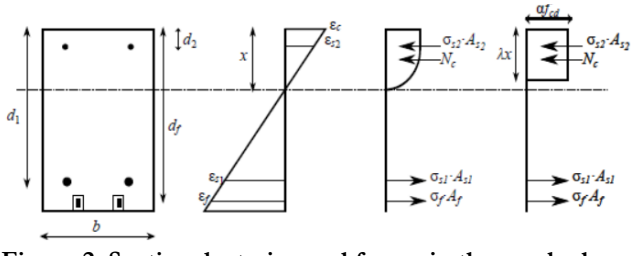

Figure 2. Sectional strains and forces in the cracked section

In Table 3, the theoretical ultimate capacity of each specimen, in terms of ultimate moment ($M_{u,theo}$), ultimate load ($P_{u,theo}$), and failure mode (FM_{theo}), is shown together with the experimental results, in terms of ultimate moment ($M_{u,exp}$), yielding load ($P_{y,exp}$), ultimate load ($P_{u,exp}$) and failure mode (FM_{exp}).

Table 3 Theoretical predictions and experimental results

		Theoretical predictions			Experimental results				$P_{u,exp}/P_{u,theo}$
	Specimen	$M_{u,theo}$ (kNm)	$P_{u,theo}$(kN)	FM_{theo}	$M_{u,exp}$ (kNm)	$P_{y,exp}$ (kN)	$P_{u,exp}$ (kN)	FM_{exp}	
S-1	**R**	11.23	44.91	SY+CC	12.05	42.00	48.20	SY+CC	1.07
	C1-1L	15.74	62.96	FRP-R	13.83	50.00	55.30	BF	0.88
	C1-2L	20.10	80.39	FRP-R	14..13	56.50	64.80	BF	0.81
	C1-4L-2G	25.62	102.46	CC	19.18	65.80	76.70	BF	0.75
	C1-4L-3G	25.58	102.32	CC	18.58	67.20	74.30	BF	0.73
	C2-1L	21.39	85.57	CC	15.37	53.50	61.50	BF	0.72
	C2-2L	26.67	106.66	CC	20.71	71.80	82.80	BF	0.78
	C3-3L	30.25	120.99	CC	17.23	64.60	68.90	BF	0.57
	C1-1B8	24.46	97.83	CC	17.18	58.00	68.70	BF	0.70
	G1-1B8	22.55	90.19	CC	14.55	50.30	58.20	BF	0.65
	C1-2B8	24.48	97.92	CC	19.30	75.30	77.20	BF	0.79
	G1-2B8	22.65	90.59	CC	17.43	59.70	69.70	BF	0.77
S-2	**CB**	27.64	69.10	SY+CC	28.16	64.50	70.40	SY+CC	1.02
	LB1C1	55.29	138.22	FRP-R	43.64	80.10	109.10	BF	0.79
	LB1G1	41.84	104.60	CC	39.68	73.70	99.20	BF	0.95
	LB2C1	70.07	175.18	CC	46.88	100.50	117.20	BF	0.67
	LB2G1	51.09	127.72	CC	44.88	82.30	112.20	BF	0.88
	LA2C1	70.07	175.18	CC	45.80	94.80	114.50	BF	0.65
	LA2G1	51.09	127.72	CC	44.24	81.70	110.60	BF	0.87
	LB1G2	52.27	130.68	CC	33.48	83.70	105.80	BF	0.81
S-3	**LB2S1**	56.93	142.32	CC	52.93	87.40	111.70	BF	0.78
	LB2S2	69.98	174.96	CC	47.40	87.30	118.50	BF	0.68
S-4	**R1**	11.15	31.86	SY+CC	10.81	28.60	30.90	SY+CC	0.97
	S1-2F	19.99	57.12	FRP-R	20.47	38.30	58.50	FRP-R	1.02
	S1-4F	27.79	79.39	CC	25.62	45.20	73.20	BF	0.92
	R2	26.23	74.93	SY+CC	26.67	73.10	76.20	SY+CC	1.02
	S2-2F	33.29	95.12	CC	34.48	81.90	98.50	CC+ BF	1.04

SY: steel yielding, FRP-R: FRP rupture, CC: concrete crushing, BF: premature bond failure

As expected, RC beams without any reinforcement (beams R, CB, R1 and R2) present an experimental yielding load close to the ultimate load, and the failure mode in all cases is the yielding of steel followed by crushing of concrete. In these cases, the ratio $P_{u,exp}/P_{u,theo}$ ranges between 0.97 and 1.07, proving that the theoretical sectional analysis provides an adequate prediction of the ultimate load.

On the other hand, regarding the beam specimens strengthened with NSM FRP, only beam S1-2F failed by FRP rupture, as it was predicted by the theoretical predictions. The rest of specimens failed before arriving at their theoretical flexural capacity, due to premature

failure by debonding of the FRP or concrete cover separation. It is therefore observed that it is of outmost importance being able to predict the flexural capacity of NSM FRP RC beams taking into account debonding failure mode.

4. Prediction models for the ultimate load considering flexural debonding

In this section, three prediction models considering flexural debonding are analysed and their results are compared to the experimental values: the American design guideline ACI 440.2R-17[6], the formulation proposed by Zilch et al. [9] and the Canadian code CSA S806-12 [8].

4.1 ACI 440.2R-17 [6]

According to the American design guideline ACI 440.2R-17, the maximum strain in the FRP reinforcement can be affected by different factors, such as the element dimensions, the reinforcement ratio or the surface coating, and can vary between $0.6\varepsilon_{fu}$ and $0.9\varepsilon_{fu}$, where ε_{fu} is the ultimate design strain of the FRP. In those cases where there is no more data, a mean value of $0.7\varepsilon_{fu}$ can be considered.

On the other hand, the FRP reinforcement needs to ensure an embedded length that has to be higher than a development length (l_{db}), defined as the minimum length needed to achieve the maximum stress in the reinforcement (Eq. (1) for circular bars and Eq. (2) for rectangular strips):

$$l_{db} = \frac{d_b}{4\tau_b} \cdot f_{fd} \quad (1)$$

$$l_{db} = \frac{a_b \cdot b_b}{2(a_b + b_b)\cdot \tau_b} \cdot f_{fd} \quad (2)$$

where a_b and b_b are the smaller and the larger cross-sectional dimensions of the FRP reinforcement, f_{fd} is the design stress of the FRP reinforcement and τ_b is the average bond strength of the joint FRP-adhesive-concrete. According to ACI 440, τ_b can be assumed as $0.5\cdot\tau_{max}$, provided that a bilinear bond-slip is considered. The parameter f_{fd} is defined in ACI 440 as the design stress of the FRP reinforcement. In this work, two different interpretations of f_{fd} (named here f_f) have been assumed, both of them calculated using sectional analysis at the maximum capacity of the element experimentally attained: i) at the section where the bending moment is maximum ($x=L_1$), ii) at the section where the moment equals to the yielding moment of the unstrengthened section ($x=x_1$).

The results according to ACI 4402-17 are presented in Table 4, in terms of:

- Development length (l_{db}), calculated according to Eqs. (1) and (2), and assuming a mean value of τ_b equal to 6.9MPa, as reccomended by ACI-440.2R for the case that no data regarding the adhesive is provided;
- Actual ancorage length (l_{act}), calculated as x minus the distance from support to the bonded FRP reinforcement (a) and taking into account the shifted tensile force envelope (a_1) due to shear effects:

$$l_{act} = x - a_1 - a \quad (3)$$

- Actual bond strength calculated according to Eqs. (1) and (2), and assuming that the development length equals to l_{act}.

Additonally, for the case of $x=x_1$, the value of x_1 is also provided. The "shift rule" is calculated according to DIN EN 1992-1-1 [14], to be consistend with the prediction model presented in Section 4.2, so a_1 is calculated as:

$$a_1 = z \cdot \frac{cot(\theta) - cot(\alpha)}{2} \quad (4)$$

In Eq. (4), z, is the mechanical lever arm, assumed as $0.9d$, being d the effective depth, θ is the strut angle calculated following Eq. (5) and α is the angle between the shear reinforcement and the member's axis.

$$1 \le cot(\theta) \le \frac{1.2}{1-V_{Rd}/V_{Ed}} \quad (5)$$

In Eq. (5), V_{Rd} is the shear resistance and V_{Ed} is the design shear force. In this study, V_{Rd} is calculated according to DIN EN 1992-1-1 [14] as:

$$V_{Rd} = c \cdot 0.48 \cdot f_{ck}^{1/3} \cdot b_w \cdot z \quad (6)$$

where c equals to 0.5, f_{ck} is the characteristic concrete strength, and b_w is the width of the specimen.

Table 4 Theoretical predictions according to ACI 440.2R-17

			At $x=L_1$					At $x=x_1$				
	Specimen	cot(θ)	a_1 (mm)	f_f (MPa)	l_{db} (mm)	l_{act} (mm)	τ_{act} (MPa)	f_f (MPa)	l_{db} (mm)	x_1 (mm)	l_{act} (mm)	τ_{act} (MPa)
S-1	**C1-1L**	2.47	163	1295	115	187	4.3	451	40	387	74	3.8
	C1-2L	1.97	129	1232	110	221	3.4	420	37	330	51	5.1
	C1-4L-2G	1.75	115	980	87	235	2.6	359	32	279	14	29.1
	C1-4L-3G	1.75	115	916	81	235	2.4	361	32	288	23	12.4
	C2-1L	1.92	126	992	166	224	5.1	436	73	348	72	7.0
	C2-2L	1.72	114	1086	182	236	5.3	366	61	258	-5	-
	C3-3L	1.63	107	522	87	243	2.5	321	54	311	53	6.9
	C1-1B8	1.79	117	836	242	233	7.2	364	105	311	44	16.5
	G1-1B8	2.13	140	461	73	210	4.4	167	43	368	78	4.3
	C1-2B8	1.63	107	576	320	243	4.7	290	105	277	20	29.1
	G1-2B8	1.87	123	442	122	227	3.7	147	43	307	34	8.8
S-2	**LB1C1**	2.06	219	1376	399	381	7.2	433	126	480	61	14.1
	LB1G1	2.68	285	1015	294	315	6.4	186	54	528	44	8.5
	LB2C1	1.79	190	847	246	410	4.1	362	105	447	57	12.7
	LB2G1	2.19	233	732	212	367	4.0	171	50	467	34	10.0
	LA2C1	1.79	190	804	233	410	3.9	362	105	458	68	10.7
	LA2G1	2.19	233	705	204	367	3.8	171	50	474	41	8.3
	LB1G2	2.15	228	569	247	372	4.6	166	72	495	67	7.4
S-3	**LB2S1**	2.01	214	1318	209	386	3.7	414	66	469	55	8.2
	LB2S2	1.79	190	798	76	410	1.3	340	32	442	53	4.2
S-4	**S1-2F**	2.67	175	2269	202	375	3.7	420	37	363	38	6.8
	S1-4F	1.99	131	1789	159	419	2.6	361	32	290	10	22.5
	S2-2F	1.79	118	2119	189	432	3.0	486	43	518	251	1.2

It is observed that the development length (l_{db}) calculated on the basis of a fixed shear stress of 6.9 MPa (as mentioned before) is lower at x_1 than at L_1. This is because at x_1 the tensile stress at the NSM FRP (f_f) is lower than at L_1, so according to Eqs. (1) and (2) lower values of l_{db} are expected at x_1.

Moreover, in general, at x_1 the calculated development length is higher than the actual anchorage length, meaning that at failure, ACI predicts a higher anchorage length than actually provided. On the contrary, at L_1 the development length is lower than the actual anchorage length, indicating the opposite behaviour than at x_1.

Finally, it is observed that at $x=L_1$, the mean value of the actual shear stress considering the experimental ultimate moment (column $\tau_{act}(L_1)$ in Table 4) is 4.1 MPa. This parameter represents the theoretical value of

the shear strength acting in the FRP-concrete joint at the failure load, and in this case lies in between the limits indicated by the ACI (i.e. 3.5 to 20.7 MPa), although it is lower than the recommended value (6.90 MPa). Conversely, at the same experimental ultimate moment, at $x=x_1$, the mean value for the actual shear strength (Table 4) is $\tau_{act}(x_1)$=10.8 MPa, higher than $\tau_{act}(L_1)$ and considerably higher than 6.90 MPa. The explanation for this difference in results may lie in the fact that at x_1, the actual anchorage length l_{act} is significantly lower than at L_1, giving higher values for the actual shear strength at x_1, although at that section, the tensile stress at the NSM FRP (f_f) is lower than at L_1.

4.2 Zilch et al. 2014 [9]

According to the formulation presented by Zilch et al. [9], the end anchorage needs to be checked at the point where the strip is no longer required for the load-carrying capacity. Hence, the anchorage of a NSM FRP strip needs to be verified at the point at which the FRP strip is first required for load-bearing purposes. This point has been assumed to be the one at which the moment equals the yielding moment of the unstrengthened section ($M_{y,unstr}$) taking into account the "shift rule", as in the previous section [9]. At that point, the resulting value of the bond capacity per FRP strip (F_b, tensile force in the NSM reinforcement), is calculated following Eq. 7 if $l_{bL} \leq 115$mm and Eq. 8 if $l_{bL} > 115$mm:

$$F_b = b_L \cdot \tau_b \cdot \sqrt[4]{a_r} \cdot l_{bL} \cdot (0.4 - 0.0015 l_{bL}) \cdot 0.95 \quad \textbf{(7)}$$

$$F_b = b_L \cdot \tau_b \cdot \sqrt[4]{a_r} \cdot \left(26.2 + 0.065 \cdot tanh\left(\frac{a_r}{70}\right) \cdot (l_{bL} - 115)\right) \cdot 0.95 \quad \textbf{(8)}$$

In Eq.s (7) and (8), b_L is the height of the strips, τ_b is the bond strength, assumed to be the minimum between the concrete bond strength and the adhesive bond strength, a_r is the edge distance of the strip, and l_{bL} is the available bond length, equal to l_{act} of the previous section.

The parameter τ_b has been assumed to be the bond strength of the adhesive, and has been calculated according to the Mohr-Coulomb failure criterion given by the tensile strength f_{Gtk} and the compressive strength f_{Gck}, as:

$$\tau_b = k_{sys} \cdot \sqrt{\left(2f_{Gt} - 2\sqrt{(f_{Gt}^2 + f_{Gc}f_{Gt})} + f_{Gc}\right) \cdot f_{Gt}} \quad \textbf{(9)}$$

In Eq. (9), k_{sys} is a system coefficient ranging between 0.6 and 1.0, and considered equal to 0.8 in this study.

As in the previous section, the theoretical total tensile force is calculated at the maximum experimental load at two different locations: $x=L_1$ and $x=x_1$. The total force $F_{b,tot}$ is obtained by multiplying the tensile force F_b calculated by Eqs. (7) and (8) by the number of grooves of the NSM reinforcement. This force is compared with the actual tensile force in the NSM reinforcement (F_{Ed}), calculated according to sectional analysis at the maximum experimental load. Results are shown in Table 5.

As expected, the total tensile force that can withstand the NSM reinforcement according to Zilch methodology ($F_{b,tot}$) is higher at L_1 than at x_1, as it is the actual tensile force. For this reason, a force ratio (FR) between both forces can be defined as $F_{b,tot}/F_{Ed}$. If FR is higher than 1, the tensile force in the NSM reinforcement predicted by this formulation is higher than the actual force in the NSM FRP at the experimental failure, meaning that the specimen failed before predictions. By contrast, FR lower than 1 means that the methodology is conservative and beams withstood more load than the expected one. At x_1, the mean value of FR is 0.75, whilst at L_1 the mean value is 0.53. It is observed that in both cases, the methodology generally gives a conservative result of the maximum tensile force that can withstand the FRP reinforcement, being more close to the experimental values at x_1 than at L_1.

Table 5 Theoretical predictions according to Zilch et al. and CSA S806-12

		Zilch et al.					CSA S806-12	
			At $x=L_1$		At $x=x_1$		$P_{u,CSA}$ (kN)	$P_{exp}/P_{CSA-S806}$
	Specimen	τ_b (MPa)	$F_{b,tot}$ (MN)	F_{Ed} (MN)	$F_{b,tot}$ (MN)	F_{Ed} (MN)		
S-1	**C1-1L**	18	14.5	18.1	10.5	6.4	53.63	1.03
	C1-2L	18	26.9	34.5	14.7	11.8	62.79	1.03
	C1-4L-2G	18	27.4	54.9	4.6	20.1	81.47	0.94
	C1-4L-3G	18	37.1	51.3	10.4	20.2	81.33	0.91
	C2-1L	23	19.7	29.8	13.1	13.1	65.25	0.94
	C2-2L	23	34.7	65.2	0	22.0	86.35	0.96
	C3-3L	23	47.3	46.9	26.9	28.9	106.15	0.65
	C1-1B8	23	16.0	42.0	7.4	18.3	76.51	0.90
	G1-1B8	18	12.2	23.2	8.7	8.4	69.17	0.84
	C1-2B8	23	28.0	57.9	6.6	29.1	76.60	1.01
	G1-2B8	18	21.7	42.4	8.4	14.8	69.58	1.00
S-2	**LB1C1**	20	18.0	69.2	8.4	21.8	103.23	1.06
	LB1G1	20	16.5	51.0	6.5	9.3	80.85	1.23
	LB2C1	20	31.1	85.2	14.5	36.4	138.16	0.85
	LB2G1	20	29.7	73.5	9.7	17.2	94.41	1.19
	LA2C1	23	37.0	80.9	19.4	36.4	138.16	0.83
	LA2G1	23	21.0	70.9	7.4	17.2	94.41	1.17
	LB1G2	20	26.7	64.3	13.5	18.8	97.31	1.09
S-3	**LB2S1**	20	37.9	73.8	17.8	23.2	106.01	1.05
	LB2S2	20	77.9	89.4	34.1	38.1	142.14	0.83
S-4	**S1-2F**	18	32.1	63.5	11.6	11.8	44.66	1.31
	S1-4F	18	33.6	100.2	3.4	20.2	57.79	1.27
	S2-2F	18	34.0	59.3	27.9	13.6	86.65	1.14

4.3 CSA S806-12 [8]

The Canadian standard CSA S806-12 does not provide specific formulations to prevent FRP debonding failure. However, the maximum strain in the NSM reinforcement is limited to 0.007 and limitations on the mechanical properties of the FRP composite are enforced.

The ultimate bending load calculated following Canadian Code ($P_{u,CSA}$) is shown in Table 5. It is observed that limiting the maximum strain in the NSM reinforcement to 0.007, although it is a simple approach, provides a good fit to the experimental results, with a mean ratio between the experimental and the predicted load of 1.01.

4.4 Comparison between ACI and Zilch et al. prediction models

In this section, the results of prediction models of ACI 440.2R and Zilch et al. methodologies are compared at the location where the NSM reinforcement is first needed (x_1). The theoretical shear stress calculated according to ACI 440.2R (τ_{act}, Table 4) versus FR defined in the previous section (Table 5) is plotted in Figure 3. Additionally, two reference lines are included in the figure: i) a vertical line indicating the mean value for the shear stress

recommended in ACI (τ_{act} =6.9MPa) and ii) an horizontal line representing FR=1.0. The intersection between the horizontal and vertical line indicate the point of perfect fit between experimental results and theoretical predictions.

Following these two lines, four quadrants can be defined. Points located at quadrant I (τ_{act},>6.9MPa, FR>1) indicate that, at failure, according to ACI 440 [6] the resin is working at a shear stress bigger than the recommended, but according to [9], the theoretical tensile force in the NSM reinforcement is higher than the experimentally obtained. As it can be observed, no specimens have followed this combination.

A similar trend is observed in quadrant III (τ_{act},<6.9MPa, FR<1): no specimens have followed a theoretical shear stress according to ACI lower than 6.9MPa and at the same time, their theoretical tensile force calculated following [9] results lower than the experimental one.

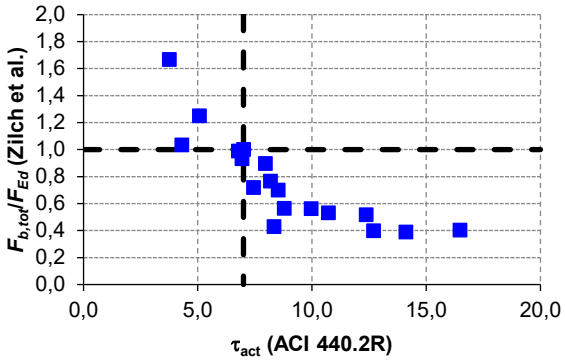

Figure 3. Comparison between ACI 440.2R and Zilch et al. prediction models

Quadrant II indicates that the specimen has failed at a lower load than the expected one according to both methodologies, and it is observed that only 3 specimens follow this trend. Finally, the majority of specimens are located in quadrant IV, which indicates that both ACI and Zilch methodologies underpredict the maximum experimental load, or, in other words, the specimens withstood more load that the predicted one.

To sum up, it can be concluded that, in general, a relevant majority of the experimental results analysed in this work are in the side of safety for both methodologies.

5. Conclusions

This paper presents the results of 27 reinforced concrete beams strengthened with NSM FRP reinforcement tested at the University of Girona. The results, in terms of maximum load capacity, yield load and failure mode are compared with a cracked sectional analysis, obtaining that, in general, almost all beams failed by debonding or concrete cover separation of the NSM FRP from the concrete element.

The experimental results are then compared with three different approaches found in the literature related to debonding failure of flexural reinforced concrete elements strengthened with NSM FRP, obtaining the following conclusions:

- Limiting the maximum strain in the NSM reinforcement to 0.007, as suggested by CSA S806-12 gives a good fit to the experimental results, although this methodology does not consider any other parameter.
- ACI 440.2R-17 provides a methodology to compute the development length (l_{db}), defined as the minimum length needed to achieve the maximum stress in the reinforcement. It is observed that, at the point where the NSM strengthening is first required (x_1), the actual anchorage length is generally lower than the development length calculated by ACI. Moreover, if the actual bond stress is calculated at failure also at x_1, a generally high value of the bond shear stress is obtained, indicating that beams withstood more load than the one expected according to ACI.
- Zilch et al. provide a methodology to calculate the bond capacity of FRP strips so as to avoid debonding of the NSM FRP reinforcement. This methodology is compared to the tensile force at the NSM

FRP reinforcement at failure, observing that the majority of specimens present a tensile force lower than the one provided by calculations.

- Both ACI and Zilch et al. methodologies can predict with a certain safety margin the debonding failure of NSM FRP RC beams.

Acknowledgments

The authors acknowledge the support provided by the Spanish Government (MINECO), Project Ref. BIA2017-84975-C2-2-P. The third author acknowledges the grant 2019-FI-B-00054.

References

[1] Bank LC. Composites for Construction: Structural Design with FRP Materials. John Wiley & Sons, Inc.; 2006. doi:10.1002/9780470121429.

[2] Teng J, Chen JF, Smith S, Lam L. FRP Strengthened RC Structures. John Wiley & Sons, Inc.; 2001. doi:10.1002/pi.1312.

[3] FIB. Externally bonded FRP reinforcement for RC structures. vol. 14. Lausanne, Switzerland: 2001.

[4] De Lorenzis L, Teng JG. Near-surface mounted FRP reinforcement: An emerging technique for strengthening structures. Compos Part B Eng 2007;38:119–43. doi:10.1016/j.compositesb.2006.08.003.

[5] Sena-Cruz JM, Barros JAO. Bond between Near-surface mounted carbond-fiber reinfroced polymer laminate strips and concrete. J Compos Constr 2004;8:519–27.

[6] ACI Commitee 440. ACI 440.2R-17. Guide for the design and construction of externally bonded FRP systems for strengthening concrete structures. vol. 24. Farmington Hills, Mich., USA: 2017. doi:10.1061/40753(171)159.

[7] CNR. Guide for the design and construction of externally bonded FRP systems for strengthening existing structures. 2013.

[8] Canadian Standards Association. CAN/CSA-S806-12. Design and construction of building structures with fibre-reinforced polymers 2012:206.

[9] Zilch, Konrad; Niedermeier, Roland; Finckh W. Strengthening of Concrete Structures with Adhesively Bonded Reinforcement. Berlin (Germany): Ernst & Shon; 2014.

[10] Sharaky IA, Torres L, Comas J, Barris C. Flexural response of reinforced concrete (RC) beams strengthened with near surface mounted (NSM) fibre reinforced polymer (FRP) bars. Compos Struct 2014;109:8–22. doi:10.1016/j.compstruct.2013.10.051.

[11] Sharaky IA, Torres L, Sallam HEM. Experimental and analytical investigation into the flexural performance of RC beams with partially and fully bonded NSM FRP bars/strips. Compos Struct 2015;122:113–26. doi:10.1016/j.compstruct.2014.11.057.

[12] Moawad M, Torres L, Barris C, Baena M, Emara M, Perera R. Sustained loading effects on NSM strengthened RC beams with different CFRP ratios. Adv. Compos. Constr. ACIC 2017 - Proc. 8th Bienn. Conf. Adv. Compos. Constr., 2017.

[13] Comité Europeen de Normalisation. Eurocode 2: Design of concrete structures: Part 1-1: General rules and rules for buildings 2004:225.

[14] Comité Europeen de Normalisation. Nationaler Anhang - National festgelegte Parameter - Eurocode 2: Bemessung und Konstruktion von Stahlbeton - und Spannbetontragwerken - Teil 1-1: Allgemeine Bemessungsregeln und Regein für den Hochbau 2013.